

# Analysis of flat fluorescent lamp discharges for LCD backlight unit by using two-dimensional fluid simulation code

Hyun Jin Yoon<sup>1</sup>, Chang Seung Ha<sup>1</sup> and Hae June Lee<sup>1</sup>

<sup>1</sup>Dept. of Electrical Engineering, Pusan National University, Busan 609-735, Korea

TEL:82-51-510-3516, e-mail: h-yoon@pusan.ac.kr.

**Keywords :** LCD backlight unit, two-dimensional simulation, flat fluorescent lamp

## Abstract

A two-dimensional fluid simulation code has been developed in order to investigate discharge phenomena and to improve plasma luminous efficiency in a Hg flat fluorescent lamp (FFL) for an LCD backlight unit. In this study, the method of a two-dimensional fluid simulation for FFL is explained and the simulation results of Hg-Ar-Ne mixture gas are presented for the enhancement of the luminance efficiency. The effects of various parameters, such as driving voltage, frequency, and gas mixture ratio, are investigated. The luminance efficiency increased with increasing fraction of mercury but the increasing fraction of argon did not affect the efficiency much.

## 1. Introduction

For the purpose of uniform light generation, external electrode fluorescent lamps (EEFLs) [1-3] have been developed as a replacement of the internal electrode of CCFLs [4]. But these lamps are not suitable for LCD TVs which have diagonal size larger than 42 inch because of poor luminance uniformity and slow response time. In a large size backlight unit (BLU), the structure becomes complicated. Flat fluorescent lamps (FFLs) have been developed in order to simplify the structure and reduce the production cost of a large size BLU since late 1990s [5-7].

In this paper, a two-dimensional fluid simulation of a flat fluorescent lamp (FFL) with Hg-Ne-Ar gas mixtures is introduced for the development of high-efficiency backlight units (BLU) for LCD TV. The simulation results are presented in Sec. 3 for a Hg-Ar-Ne mixture gas by using two-dimensional fluid code. The simulation is carried out to investigate plasma (electron and ion) and neutral particle densities. It gives insight into how to get high luminance efficacy Hg plasma for a large size LCD backlight unit.

## 2. Model description

In the two-dimensional fluid simulation of FFL, the plasma behavior is described with the continuity equations of electrons, ions and neutrals. For each step, the number density  $n_i$  is calculated from a continuity equation as below

$$\frac{\partial n_i}{\partial t} + \nabla \cdot \bar{\Gamma}_i = S_i \quad (1)$$

where  $n_i$ ,  $\bar{\Gamma}_i$ , and  $S_i$  are the number density, the particle flux, and the source term for each species, respectively. For the momentum conservation equation, the drift-diffusion approximation is used to simplify the particle flux :

$$\bar{\Gamma}_i = \pm \mu_i n_i \bar{E} - D_i \nabla n_i \quad (2)$$

where the plus and minus sign means the sign of the charged particles (+ for positive and - for negative species),  $\mu_i$  is the mobility, and  $D_i$  is the diffusion coefficient, and  $\bar{E}$  is electric field. For the calculation of rate coefficients, the Local Field Approximation (LFA) is used to calculate the collision parameters as a function of the electric field intensity divided by gas pressure (E/p), by using BOLSIG code [8-9]. Equations (1) and (2) require the input of mobilities, diffusion coefficients, and reaction rate coefficients. In general, these quantities depend on the energy distribution of the considered particles. To calculate the electric field, we used Poisson's Equation,

$$\nabla \cdot \bar{E}_s = -\nabla^2 \Phi = \frac{\rho}{\epsilon_0} \quad (3)$$

where  $\epsilon_0$  is the dielectric permittivity.

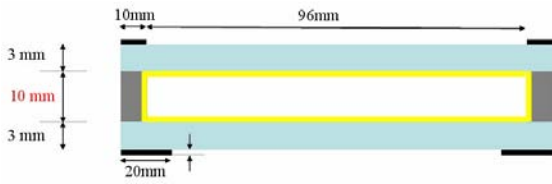


**Fig. 1 FFL cell structure for two-dimensional simulation model considered in the calculations.**

Figure 1 shows the test simulation domain of the structure of an FFL in a two-dimensional region. The FFL plasma discharge is generated inside two dielectric glasses with thickness 3mm, and closed barrier ribs whose height varies by a few mm. There are four electrodes on each outside surface of the glasses where sinusoidal voltage is applied. The parameters are not exactly the same as those used in commercial devices, but this simplified geometry gives a lot of information about FFL discharges.

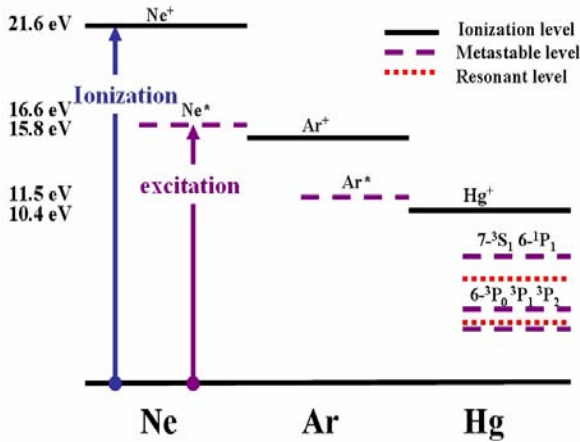


**Fig. 2 Energy diagram for Ne, Ar, and Hg. Solid line, dashed line and dotted line indicates ionization, meta stable, and resonant state energy level, respectively**

Figure 2 shows the Grotian diagram of Ar, Ne, and Hg. The ionization energies of Ne, Ar, and Hg are 21.6, 15.8 and 10.4 eV and the electron impact excitation energies are 15.8, 11.5, and 4.67 eV, respectively. The most important species is Hg in Ar-Ne-Hg mixtures. Hg <sup>3</sup>P<sub>1</sub> and <sup>1</sup>P<sub>1</sub> excited state species which have the excitation energies of 4.89 and 6.7 eV emit ultraviolet (UV) radiation with wavelengths of 254 nm and 185 nm, respectively. Especially Hg <sup>3</sup>P<sub>1</sub> excited state plays an important role in radiation

because of the low threshold energy in Fig. 2. Hg excited state species are generated by low energy electrons and Hg<sup>+</sup>, Ar<sup>+</sup>, and Ne<sup>+</sup> are generated by high energy electron in the sheath.

As shown in Table 1, the reaction rate coefficients of electron-Hg, electron-Ne, electron-Ar, and heavy particle collisions are summarized. The main route to make charged particles is by electron impact ionization and does not involve step ionization. The ions and electrons are also increased by the excited neutral states of Ne, Ar, and Hg collisions and the reaction rate coefficients are calculated by the zero-dimensional Boltzmann equation.

**TABLE 1. Reaction rate coefficients of electron impact collisions with Ar, Ne, and Hg, and heavy particle collisions.**

Electron impact excitation	Rate coefficient
$e + \text{Hg} \rightarrow \text{Hg}^f (6^1\text{P}_1) + e$	a
$e + \text{Hg} \rightarrow \text{Hg}^f (6^3\text{P}_1) + e$	a
$e + \text{Hg} \rightarrow \text{Hg}^m (6^3\text{P}_0) + e$	a
$e + \text{Hg} \rightarrow \text{Hg}^m (6^3\text{P}_2) + e$	a
$e + \text{Hg} \rightarrow \text{Hg}^{**} + e$	a
$e + \text{Ar} \rightarrow \text{Ar}^* + e$	a
$e + \text{Ne} \rightarrow \text{Ne}^* + e$	a
Electron impact ionization	
$e + \text{Ne} \rightarrow \text{Ne}^+ + e + e$	a
$e + \text{Ar} \rightarrow \text{Ar}^+ + e + e$	a
$e + \text{Hg} \rightarrow \text{Hg}^+ + e + e$	a
Heavy particle collision	
$\text{Ne}^* + \text{Hg} \rightarrow \text{Ne} + \text{Hg}^+ + e$	$6.4 \times 10^{-11} \text{ cm}^3/\text{s}$
$\text{Ar}^* + \text{Hg} \rightarrow \text{Ar} + \text{Hg}^+ + e$	$9.0 \times 10^{-10} \text{ cm}^3/\text{s}$
$\text{Hg}^* + \text{Hg} \rightarrow \text{Hg} + \text{Hg}^+ + e$	$3.5 \times 10^{-10} \text{ cm}^3/\text{s}$
$\text{Ne}^* + \text{Ne} \rightarrow \text{Ne} + \text{Ne}^+ + e$	$1.0 \times 10^{-11} \text{ cm}^3/\text{s}$
$\text{Ar}^* + \text{Ar} \rightarrow \text{Ar} + \text{Ar}^+ + e$	$5.0 \times 10^{-10} \text{ cm}^3/\text{s}$

<sup>a</sup> Rate coefficients have units of (cm<sup>3</sup>/s) unless otherwise noted and are calculated from the BOLSIG code<sup>[8-9]</sup> using cross-sections according to each reaction.

### 3. Results and discussion

Figure 3 shows the charged particles (Ne<sup>+</sup>, Ar<sup>+</sup>, Hg<sup>+</sup>, and electron) and excited neutrals (Hg <sup>3</sup>P<sub>1</sub> and Hg<sup>1</sup>P<sub>1</sub>) density profiles during one cycle. The

simulation was carried out with a pressure of 30 Torr, a Hg ratio of 1.4 %, an Ar ratio of 5 %, a driving frequency 10 kHz, and a driving voltage of 1 kV. Positive ion ( $\text{Ne}^+$  and  $\text{Ar}^+$ ) densities are distributed at the end of the discharge region, and electrons travel to the positive column region because of the strong electric field in the sheath near electrodes. Otherwise,  $\text{Hg}^+$  ions are distributed uniformly inside the positive column where the electric field is low.  $\text{Hg}^*(^3\text{P}_1)$  and  $\text{Hg}^*(^1\text{P}_1)$  excited state neutrals are created by electron impact collisions inside the positive column region. Thus, the ultraviolet (UV) light reaching the phosphors makes uniform visible light in the FFL.

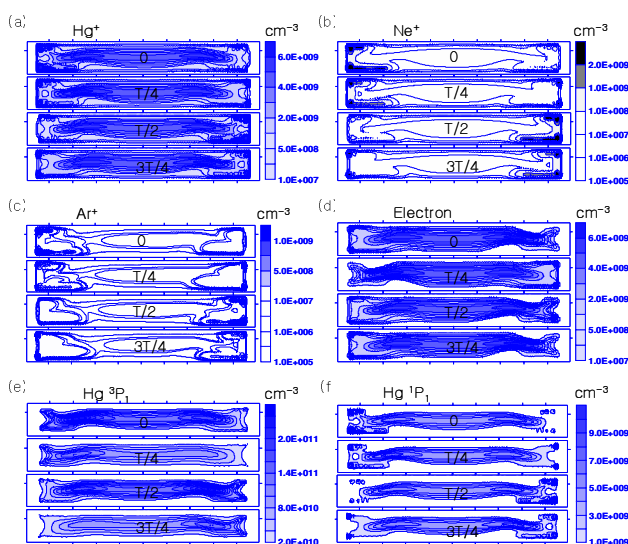


**Fig. 3.** Densities of (a) $\text{Hg}^+$ , (b) $\text{Ne}^+$ , (c) $\text{Ar}^+$ , (d)electrons, (e) $\text{Hg } ^3\text{P}_1$ , and (f)  $\text{Hg } ^1\text{P}_1$ , respectively. (Applied voltage 1 kV, gas pressure 30 Torr, Hg-Ar-Ne gas ratio 1.4:5:93.6, and applied frequency 10 kHz)

Figure 4 shows the effect of driving voltage on luminous efficiency, luminance, electron density, and the density of the  $\text{Hg } ^3\text{P}_1$  excited state. The driving voltage is sinusoidal with frequency of 10 kHz, and the background pressure is 30 Torr. The discharge efficiency increases along with the driving voltage, since the high electric field then makes more plasma (electrons and ions) and the  $\text{Hg } ^3\text{P}_1$  excited neutrals.  $\text{Hg } ^3\text{P}_1$  contributes to generating UV radiation.

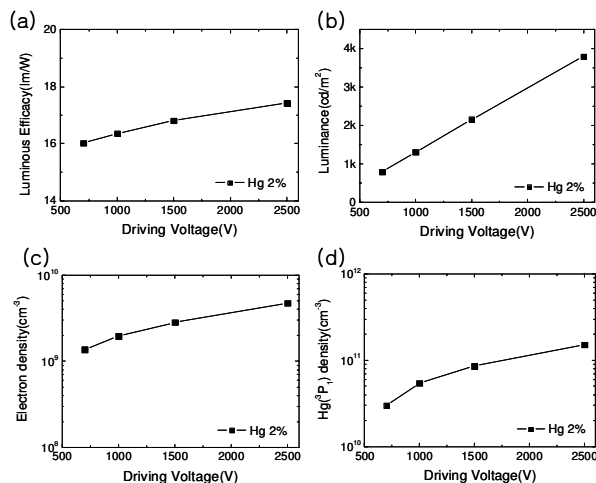


**Fig 4.** (a) Luminous efficiency, (b) luminance, (c) electron density, and (d) $\text{Hg } ^3\text{P}_1$  density as a function of driving voltage at Hg 2 %, Ar 5 %, frequency 40 kHz, and pressure 30 Torr.

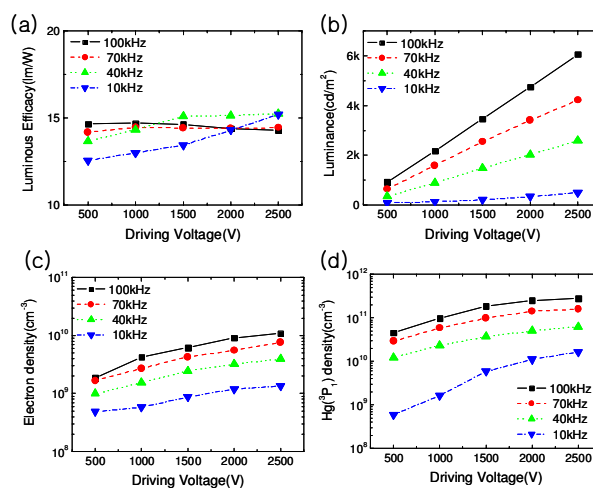


**Fig 5.** The effect of driving frequency on (a) luminous efficiency, (b) luminance, (c) electron density, and (d) $\text{Hg } ^3\text{P}_1$  density at Hg 1 %, Ar 3 %, and pressure 30 Torr.

Figure 5 shows the effect of driving frequency on luminous efficiency, luminance, electron density, and the density of the  $\text{Hg } ^3\text{P}_1$  excited state. The FFL uses a power supply with a frequency range of 10-100 kHz. Electron and  $\text{Hg } ^3\text{P}_1$  densities increase with the driving voltage and frequency in this region because more electrons can be created by the higher electric field. Thus, the luminance increases with both the

driving voltage and the driving frequency.

The luminous efficiency is affected by Hg content because the ionization process happens mainly for Hg species. The Hg  $^3P_1$  neutral density increases with the Hg concentration ratio in Fig.4 (Hg 2.0 %) and Fig. 5 (40 kHz, Hg 1.0% data). Also luminance efficiency increases with the Hg ratio. The dominant parameter which affects discharge efficiency is the content of Hg.

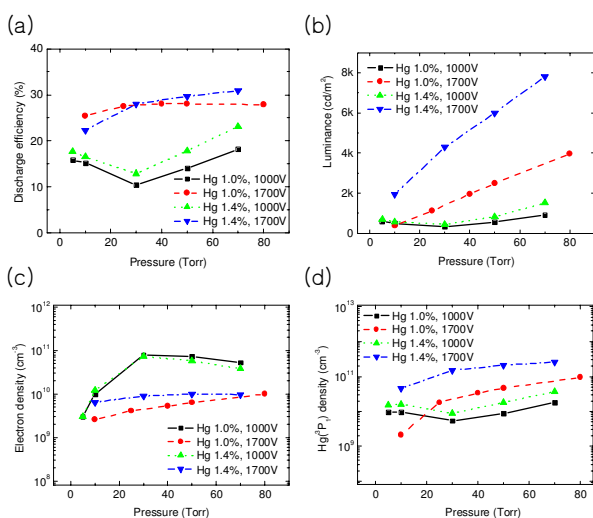


**Fig 6.** The effect of pressure on (a) the discharge efficiency, (b) luminance, (c) electron density, and (d) Hg  $^3P_1$  density at Hg 1.0 and 1.4 %, the driving voltage 1.0 and 1.7 kV, the driving frequency 40 kHz, and pressure 30 Torr.

Figure 6 shows the effect of pressure on discharge efficiency, luminance, electron density, and the density of the Hg  $^3P_1$  excited state with a pressure range 10-80 Torr. Generally, Hg  $^3P_1$  density is high in the high pressure regime, so the discharge efficiency and luminance are high in this high pressure regime. The discharge efficiency, luminance, and electron density increase with the driving voltage and gas pressure. These two parameters play important roles in making very bright and efficient FFLs.

#### 4. Summary

There is a lack of understanding of the plasma dynamics and growth mechanisms and the role of the plasma in LCD backlight units. This is because the diagnostic tools for detecting the density and other plasma parameters of the micro-plasma are poor. A two-dimensional analysis of a high pressure plasma

shows that a Hg-Ne-Ar mixture gases can be investigated by using a fluid simulation. The charged particles and excited neutrals are calculated by using fluid simulation code for the FFL.

The most dominant factor for the discharge efficiency is the Hg ratio, as the discharge efficiency increases with the Hg ratio. The luminance shows the same tendency as the Hg  $^3P_1$  excited state. The Hg  $^3P_1$  excited state neutrals increase with the applied voltage, frequency, and pressure, thus increasing luminance. Luminous efficiency mostly increased with the voltage and pressure, but there are regions where it decreased.

#### 5. References

1. T. S. Cho, H. S. Kim, Y. G. Kim, J. J. Ko, J. G. Kang, E. H. Choi, G. S. Cho, and H. S. Uhm, *Jpn. J. Appl. Phys.* **41**, 7518 (2002).
2. G. S. Cho, B. S. Kim, D. U. Yang, J. W. Hong, Y. K Lee, J. H Lee, J. Y. Lee, D. H. Lee, E. H. Choi, and J. G. Kang, *SID 3 Digest*, 1368 (2003).
3. Y. Takeda, M. Takagi, and T. Kurita, *IDW*, 2 Digest, 489 (2002).
4. R. Y. Pai, *SID 7 Digest*, 371 (1997).
5. T. Shiga, Y. Ikeda, S. Mikoshiba, and S. Shinada, *J. Lighting & Visual Environment*, **25**, 10 (2001).
6. F. Volkommer, L. Hitzchhke, *US Patent 6.034.470* (1997).
7. T. Shiga, S. Mikoshiba, J. H. Ko, K. Y. Lee, S. H. Cho, and H. T. Choi, *SID 4 Digest*, 1330 (2004).
8. J. P. Boeuf, *J. Phys. D*, 36 R53 (2003).
9. W. L. Morgan and B. M. Penetrante, *Computer Phys. Comm.*, **58**, 127 (1990).